Journal of composites science

MDPI

Article

Heat Propagation in Anisotropic Heterogeneous Polymer-CNT Composites

Ekaterina A. Vorobyeva [1,*], Nikolay G. Chechenin [1], Irina V. Makarenko [2] and Alexey V. Kepman [2]

[1] Skobeltsyn Institute of Nuclear Physics, Lomonosov Moscow State University, Leninskie Gory 1/2, Moscow 119991, Russia; chechenin@sinp.msu.ru

[2] Institute of New Carbon Materials and Technologies, Lomonosov Moscow State University, Leninskie Gory 1/11, Moscow 119991, Russia; makarenkoirina@gmail.com (I.V.M.); alexkep@inumit.ru (A.V.K.)

* Correspondence: vorkate89@mail.ru; Tel.: +7-495-939-24-53

Received: 16 June 2017; Accepted: 11 July 2017; Published: 14 July 2017

Abstract: A weak thermal conductivity (TC) of a polymer can be modified by inclusion of nanoparticles with high TC. Here we study the TC enhancement in epoxy resin (ER) based composites by incorporation of carbon nanotubes (CNTs) and demonstrate that the enhancement depends critically on the alignment of CNTs. The highest effect in TC enhancement (18.9) was obtained in ER with vertically aligned multiwall CNTs (VANTs) and in ER with horizontally aligned nanotubes (HANTs) (6.5). We analyze the influence of intrinsic structural factors of CNTs as well as extrinsic factors limiting the enhancement of the composite TC. The dynamics of heat propagation in ER/VANT, a strongly anisotropic and heterogeneous system, was studied experimentally, using laser flash apparatus (LFA), and by computer simulation, applying a coaxial cylinder model. It was found that the thermal resistivity CNT-ER interface to be a key extrinsic factor limiting the dynamics of the heat propagation. We show that these dynamics and the interface resistivity can be efficiently studied using the LFA technique.

Keywords: polymer nanocomposites; aligned carbon nanotubes; thermal conductivity; intrinsic and extrinsic factors; dynamics

1. Introduction

More than 15 years have come since the very first estimations of thermal conductivity (TC) of carbon nanotubes (CNTs). Molecular dynamic (MD) simulations predicted the maximum TC value can be as high as 37,500 W/(m·K) at T ≈ 100 K and decreased κ 6600 W/(m·K) at room temperature (RT) for isolated (10,10) single-walled CNTs (SWNTs) [1]. However, some later MD simulations showed that the resulting values depend on the size (length) of the SWNT, boundary conditions, concentration and type of defects and other conditions in calculations, resulting in a large variation in TC from 30 to 6600 W/(m·K) [2–8]. The measured TC in SWNTs are also widely scattered from 2.3 to 8000 W/(m·K) depending on the measurement method for SWNTs [9–12] and for MWNTs [13–15].

Recently developed methods of growth of arrays of vertically aligned CNTs (VANTs) can directly utilize the 1D nature of CNTs and more straight investigations of their anisotropic properties. The thermal conductivity of VANT film sandwiched between two glass plates was measured in a direct way in [16]. The value for the axial TC, κ_z, was estimated to be approximately 8.3 W/(m·K). Taking into account the presence of a significant amount of porosity in the film, the value of κ_z was considered relatively high as compared with a single CNT.

While the enhancement of electrical conductivity by an addition of CNTs accounts for many orders of magnitude [17,18], the effect in TC is much more modest. A transmission of the CNT high thermal conductivity to the polymer nanocomposite (PNC) is a challenging task requested by a large

number of applications, like heat dissipative coatings, adhesively bonded joints in micro- and powerful electronics, in aerospace and automotive industries, etc. [19]. The state-of-the-art development in the field is described in a recent review [20]. The increase in TC of a polymer composite by addition of CNTs was found to be either marginal [21], or small, up to 125% [22]. Theory predicts a highest thermal conductivity for ideal SWNTs, therefore, one would anticipate, for composites with ideal SWNTs as a filler. In practice, it is hard to grow defectless tubes on a massive production scale and, being incorporated into a polymer matrix, SWNTs can hardly conserve their virgin properties. As reported in [23], MWNTs give a larger effect in the composite TC than SWNTs.

Alignment of CNTs can give a higher enhancement in composite thermal conductivity. In the PNCs, obtained by infiltration of dense array of vertically aligned (VANTs), CNTs can provide a direct contact pathway all through the composite thickness and, hence, a high magnitude of TC. It was obtained that the effective RT thermal conductivity of the composite along the carbon nanotube alignment direction is at least 6 times larger than the thermal conductivity of the polymer matrix and 2–4 times larger than that across of aligned CNTs [24]. Densification of VANT array can further enhance the TC as shown in [25] where enhancement factor as much as 18 was achieved in PNC with 17 vol % VANTs.

In this paper, we report on the thermal conductivity measurements across the samples of epoxy resin (ER) with CNTs of different shapes and orientations, including vertically aligned (VANTs) and horizontally aligned (HANTs) MWNTs obtained by the permanent injection catalyst technique. We show that a large TC enhancement can be obtained with as-grown VANTs arrays without densification or high temperature pre-treatment before composite formation. A reasonable enhancement in TC across the sample can be achieved also in PNCs with HANTs, though not that high as in the case of PNC/VANTs. The results obtained are analyzed based on different models of heat transport in the highly heterogeneous PNC system with different intrinsic and extrinsic factors influencing the TC. The dynamics of the heat transport are simulated and discussed assuming different interfacial CNT/matrix thermal resistivity. It is shown that the dynamics of the temperature increase can be used for investigation of contact resistivity at the CNT/matrix interface.

2. Materials and Methods

2.1. CNTs Synthesis

Three types of CNTs were used to prepare PNCs: a powder of commercial nanocarbon with trade name 'taunit' [26] (TNC); randomly aligned CNTs (RANTs); and vertically aligned nanotubes (VANTs). Our SEM inspection showed that TNC-powder composed of very entangled and branching nanotubes conglomerated in micron-sized ball-like particles with a significant (up to 20%) amorphous fraction. The setup for VANTs growth has been described previously [27]. Schematically, it was a quartz tube of about 1" in diameter placed in an automatically temperature controlled oven with an automatically controlled flow rates of buffer gas (N_2). In present modification, the catalyst was injected during the growth process, like it was realized in previous studies [28,29]. The liquid solution of ferrocene, C_5H_5-Fe-C_5H_5, in cyclohexane, served as an active media, was supplied into the reactor, evaporated in a low temperature (~200 °C) zone, mixed with the support gas and passed into a high temperature zone with a preset temperature in the range of 750–950 °C where the active components decomposed. The ferrocene decomposed with iron condensed on a substrate with formation of nanoislands served as catalyst particles. The cyclohexane pyrolyzed to carbon which build-up a dense CNT forest on the catalyst layer. CNT growth regime was optimized by adjusting the flow rates of the supporting gases, flow rate of the active solution, the temperatures of the first (low) and second (high) zones, to obtain a high growth rate with the forest height of 2 mm per 1 h with a reasonable uniformity on a large area of 1.5×10 cm^2. Before further processing, the height of the array and VANTs diameter distribution were characterized using SEM. An example of a SEM-side view on VANTs forest is given in Figure 1.

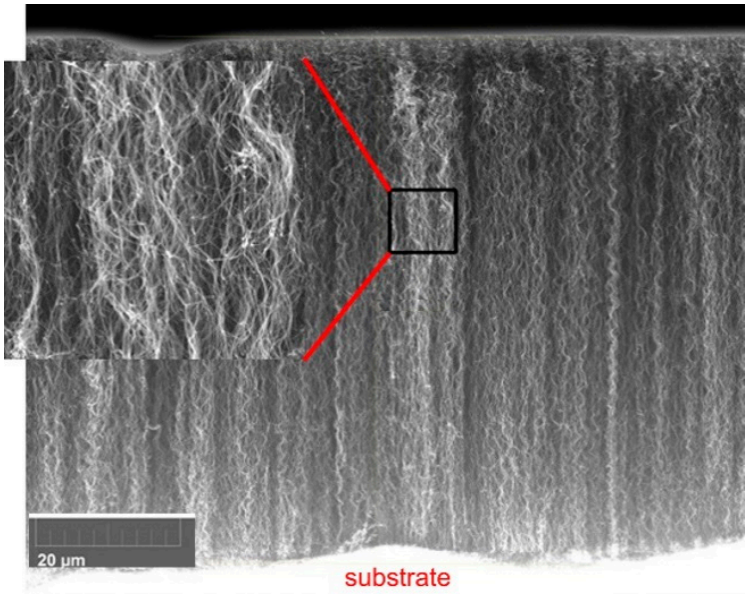

Figure 1. SEM side view on a 'forest' of nanotubes with a magnified view in the insert. The height of the forest is about 72 nm in this case.

In the current experiments, the samples with the forest height in the range of 0.5 to 2 mm and VANTs diameters of 30 to 50 nm were used. The RANTs were obtained by scraping the VANTs array from the substrate and grinding CNTs in a mortar.

2.2. PNC Sample Preparation

Epoxy based PNCs—with CNTs powder, TNC, or RANTs—were obtained by a careful mixing of a certain quantity of CNTs with a quantity of a polymer precursor to make a desirable proportion immediately after adding a hardener. The prepared mixture was left for polymerization at room temperature for about a day to finalize polymerization of the ER/TNC composite.

The samples of epoxy resin composite ER/VANTs were prepared by infiltration of liquid monomer into VANTs array, grown on Si substrate as described in the previous section. The monomer was mechanically and ultrasonically mixed with the hardener (15 wt %) and, in the amount of 10–15 wt %, with a solution of acetone and alcohol in a proportion of 3:1. In addition, to reduce the monomer viscosity and the infiltration more homogeneous, the precursor solution was heated up to 60 °C in a 5 min just prior the infiltration. The infiltrated monomer polymerized at room temperature for 24 h. The excess polymer layer on the top of the sample must be removed for further tests. For many of these tests, the substrate is also to be removed. This was normally done by mechanical grinding and polishing with a diamond paste.

Except for some important points, the preparation of ER/HANTs PNCs was the same as for ER/VANTs. Basically, the method is a reorientation of VANTs to HANTs in a liquid polymer precursor by a press-and-draw trick [18]. With such a method, a reasonable horizontal alignment of CNTs in the polymer was achieved with orientation dispersion within the sample plane of about 30°. SEM images are shown of a top view, Figure 2a, side view, Figure 2b, of a polished ER/VANTs sample and top view, Figure 2c, of ER/HANTs.

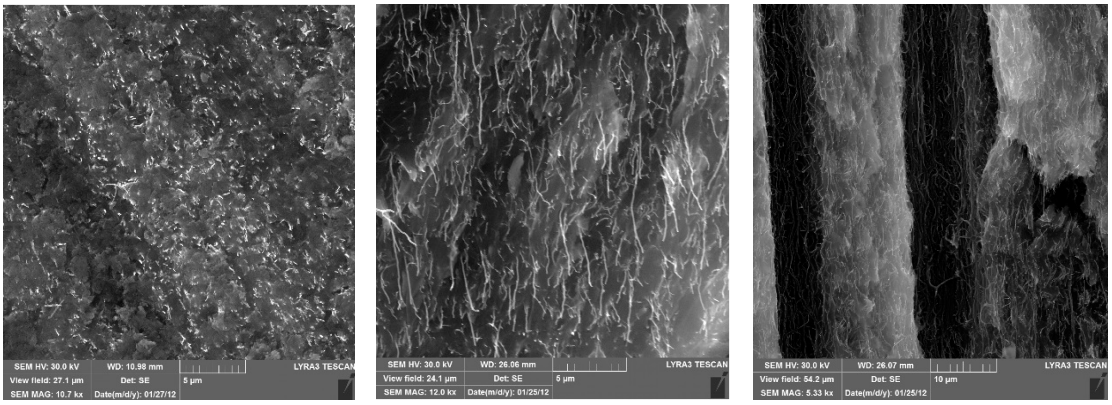

(**a**) (**b**) (**c**)

Figure 2. SEM images (**a**) top view, (**b**) side view of a polished ER/VANT sample and (**c**) top view of a polished ER/HANTs sample. The thin bright dots and lines in the images are CNTs aligned normally (a–c) parallel to the sample surface. Large scale variation of the contrast reflects the roughness of the polished top (a,c) or cracked side (b) surfaces of the samples.

The bright dots and lines in the images are CNTs aligned normally (a, b) and parallel (c) to the sample surface. One can see that alignment of CNTs is predominately preserved in the ER/VANT and nanotubes are realigned to a single direction parallel to the surface in the ER/HANT composite. As a result of the mechanical treatment, the thickness of the PNC samples was normally somewhat thinner than the original height of the VANT array and typically was in the range between 0.2 and 1.0 mm.

2.3. TC Measurements

The thermal conductivity and thermal diffusivity of the PNC samples were measured using NETZSCH LFA 457 MicroFlash apparatus in accordance with standards ASTM E-1461. The samples were cut into square shape 11 × 11 mm^2. The bottom surface of a sample under study was flushed by a laser pulse, the heat spread towards the top surface and the temperature rise as a function of time was registered by an infrared detector. A typical time dependence of the IR signal is shown in Figure 3.

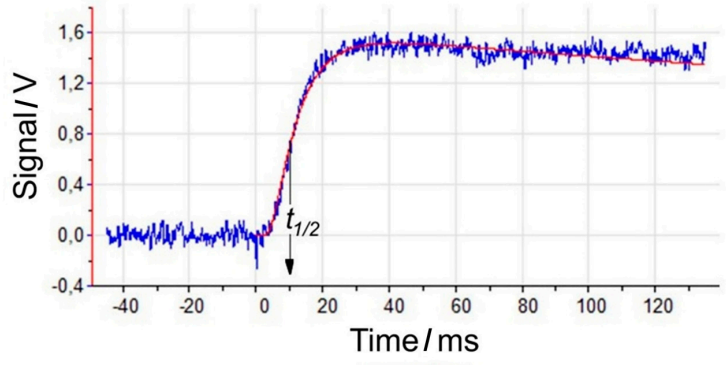

Figure 3. Time variation of LFA signal measured by IR detector corresponding to the temperature of the top surface of the sample. Blue curve—as measured for VANT + graphite sample, read curve—approximation with Cowan correction.

Assuming the uniform heat absorption induced by the laser pulse by the bottom surface of the sample, unidirectional heat propagation from bottom to the top surface, laser pulse duration much shorter than the heat propagation and absence of the energy loss, the thermal diffusivity (α) of the sample can be written as

$$\alpha = 0.139 \cdot L^2 / t_{1/2} \quad (1)$$

where L is the uniform sample thickness, $t_{1/2}$ is the rise time of the upper surface temperature to the half-maximum value. Following the Cowan model [30], the ratios of the signal rise at $5{\cdot}t_{1/2}$ and $t_{1/2}$ were determined and used for the heat loss corrections. The thermal conductivity (κ) can be determined, using the ratio

$$\kappa = \alpha{\cdot}C_p{\cdot}\rho \quad (2)$$

where ρ is the specific density and C_p is the specific heat which can be estimated by comparing the signal from the sample under investigation with that from a reference sample measured in the identical condition.

Optically transparent and reflective samples must be covered with graphite thin layer. Though all our samples were black and opaque, except the ones of pure epoxy, all our samples were covered with the graphite thickness of 5 μm, following NETZSCH Application Note recommendation [31]. To check that the graphite layer does not disturb the κ-value, the measurements of thermal conductivity were made twice for some of the samples, first for the samples as received, and then with graphite covering the surface. Both measurements gave close results, as one can see from the data in Table 1, assuring a negligible effect of graphite covering, in accordance with previous results [32]. In particular, from the comparison of the data in the third column of Table 1, it is evident that $t_{1/2}$ values are very close for both covered and uncovered samples. This holds in wide range composites with different thermal conductivities and with $t_{1/2}$ from milliseconds to seconds. The time dependence of the IR detector signal is also very alike for two type of samples, so it is undistinguishable in many cases. Additionally, repeated measurements in several days gave the same results, indicating the reproducibility of the method and its nondestructive character.

3. Results

By the method described above, the thermal conductivity, thermal diffusivity, specific heat were measured for a number of epoxy resin based composites filled with different types of carbon nanotubes. The measured conductivities, averaged over similar samples, are shown in Figure 4 and listed in Table 1.

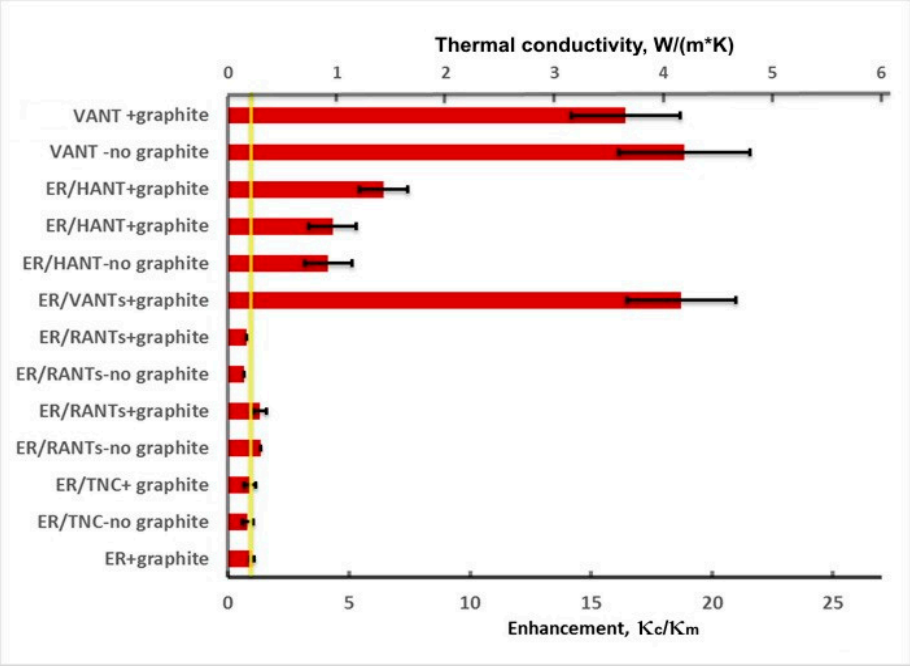

Figure 4. Thermal conductivity and enhancement for some ER-based composites filled with different types of CNTs.

Table 1. Thermal conductivity measured for a number of epoxy resin based composites filled with different types of carbon nanotubes.

Sample	L, mm	$t_{1/2}$, ms	α, mm^2/s	C_p, J/(g·K)	ρ, g/cm^3	κ_c, W/(m·K)	κ_c/κ_m
ER+graphite	1.8	4.1×10^3	0.112 ± 0.006	1.58	1.26	0.22 ± 0.02	1.0 ± 0.09
ER/TNC-no graphite	1.8	4.4×10^3	0.102 ± 0.006	1.51	1.16	0.18 ± 0.05	0.82 ± 0.23
ER/TNC+graphite	1.8	4.2×10^3	0.108 ± 0.009	1.63	1.16	0.20 ± 0.05	0.91 ± 0.23
ER/RANTs-no graphite	0.83	0.66×10^3	0.15 ± 0.001	1.89	1.107	0.30 ± 0.06	1.36 ± 0.23
ER/RANTs+graphite	0.83	0.69×10^3	0.14 ± 0.003	1.88	1.107	0.29 ± 0.06	1.32 ± 0.23
ER/RANTs-no graphite	1.83	4.8×10^3	0.097 ± 0.007	1.27	1.195	0.15 ± 0.06	0.68 ± 0.23
ER/RANTs+graphite	1.83	4.4×10^3	0.107 ± 0.009	1.36	1.195	0.17 ± 0.06	0.77 ± 0.23
ER/VANTs+graphite	0.56	13.2	3.30 ± 0.015	0.992	1.27	4.16 ± 0.50	18.9 ± 2.3
ER/HANT-no graphite	0.22	12.5	0.55 ± 0.006	1.31	0.85	0.92 ± 0.22	4.2 ± 1.0
ER/HANT+graphite	0.22	12.3	0.55 ± 0.003	1.31	0.86	0.96 ± 0.22	4.4 ± 1.0
ER/HANT+graphite	0.63	27.7	0.55 ± 0.006	2.04	0.55	1.43 ± 0.22	6.5 ± 1.0
VANT-no graphite	0.59	8.8	5.449 ± 0.133	0.885	0.87	4.19 ± 0.6	19.1 ± 2.7
VANT+graphite	0.59	10.7	4.456 ± 0.029	0.943	0.87	3.65 ± 0.5	16.6 ± 2.3

* Abbreviations: ER—pure epoxy resin, ER/TNC—ER with commercial nanocarbon "taunit", ER/RANTs, ER/VANTs and ER/HANTs—ER with randomly, vertically, and horizontally aligned nanotubes, respectively.

There was no clear dependence observed of the thermal conductivity on the CNT concentration in the loading range up to 10 wt %. The measured values for ER/TNC and ER/RANTs were the same within the error bars as for ER. A sharp increase of the thermal conductivity—by a factor of 18.9, compared with pure ER—was observed in ER/VANTs composite across the sample thickness and, hence, predominately along the MWNTs axis. This increase is close to that in [25], where the enhancement factor from 5 to 18 was demonstrated in the composites with 10% to 17% CNT volume fraction. A much higher enhancement, up to 100, was reported in [33] where the VANT array was annealed to a temperature of 2000 °C. In our approach, we used as-grown arrays—i.e., without densification and high temperature annealing—which is more economically justified for practical applications. The ER/HANT composite showed somewhat lower enhancement, by a factor of 5, in transverse thermal conductivity, i.e., the conductivity across the sample thickness and across the side surface of the MWNTs. This is again in agreement with previous observations in [25], where the transverse thermal conductivity was much smaller than the longitudinal one and was of the factor of 5 in the CNT concentration range of 13 to 17 vol % which is significantly larger than that of CNT fraction range in our composite.

The pristine array—i.e., without polymer—was also measured and presented in Table 1. One can note that the measured thermal parameters $t_{1/2}$, α, C_p, and κ_c for the VANT arrays are close to those for ER/VANT. The ratios κ_c/κ_m in the last column are artificial for VANT arrays, since the surrounding of the tubes in this case is an ambient atmosphere, i.e., air in the normal condition and not a polymer. The reason to relate the VANT array thermal conductivity to that of ER is just to have a common base for comparison. More realistic normalization is discussed in Section 4.1.

4. Discussion

4.1. Effective Medium Consideration

It follows from above that incorporation of CNTs does not automatically lead to increase in thermal conductivity of composite. The heat transport remains as low as in pure epoxy at up to and above of 10 wt % loading of entangled and randomly aligned CNTs. Similar observations have been reported in [23]. One of possible reasons for low conductivity can be misalignment and agglomeration of the CNTs, making the interparticle distance larger than in the case of fine dispersion. In the extreme case, the entangled and conglomerated CNTs lose their high aspect ratio and can be considered as spherical particle of a micron size with quite a modest contribution into TC, which we observed in ER/TNC and ER/RANTs samples, where the TC enhancement was within the error bars as reported in Table 1. Weak enhancement with randomized CNTs orientation in ER/RANTs indicate not only the reduced amount of tubes in the 'right' direction, but also a presence of tube–tube and tube–matrix contact thermal resistivities, prohibiting the percolation effect in this inhomogeneous system.

In contrast with TNC and RANTs, aligned CNTs connect bottom and top surfaces all through the thickness of the PNC sample without significant change in their high aspect ratio. Two simplest approaches which could be applied for composites with aligned CNTs are the rule of mixture and so-called series model. For vertical ER/VANTs composites, the rule of mixture assumes the parallel contribution of thermal conductivities of VANTs (κ_{nt}) and polymer matrix (κ_m) into the effective composite thermal conductivity (κ_c) in the proportion of the volume fractions of VANTs Φ and the matrix $(1 - \Phi)$

$$\kappa_c = \kappa_{nt}\Phi + \kappa_m(1 - \Phi) \tag{3}$$

The volume fraction of CNTs, Φ, can be estimated from the relation

$$\Phi = w_{nt}\rho_m/(w_{nt}\rho_m + w_m\rho_{nt}) \tag{4}$$

where w_{nt} (ρ_{nt}) and w_m (ρ_m) are the weight concentrations (mass density) of nanotubes and the matrix, respectively. Assuming the CNTs specific mass density the same as for graphite ($\rho_{nt} \approx 2$ g/cm^3), and that of epoxy ≈1.2 g/cm^3, for 5 wt % we obtain 3 vol % CNTs for VANTs, which is in agreement with estimations from direct SEM observations. Applying an average parameters for our VANT arrays, diameter CNTs 40 nm, spacing between CNTs centers 200 nm, one can obtain the CNTs volume fraction about Φ = 3 vol %. From Table 1 the measured κ_c = 4.16 W/(m·K) we get κ_{nt} = 131 W/(m·K) for an individual VANT in the composite.

A different approach for estimation of the TC in a diluted CNT composite was developed in [34], based on the effective medium theory. The composite is considered a homogeneous medium with CNT fluctuating contribution. In this case, the TC enhancement was obtained as

$$\kappa_c/\kappa_m = [3 + \Phi(\kappa_{nt}/\kappa_m)]/(3 - 2\Phi) \tag{5}$$

and κ_{nt} can be expressed as

$$\kappa_{nt}/\kappa_m = [(3 - 2\Phi)\kappa_c/\kappa_m - 3]/\Phi \tag{6}$$

Following (6) and using the measured effective enhancement of the conductivity κ_c/κ_m = 18.9, we obtain the CNTs thermal conductivity enhancement κ_{nt}/κ_m = 1850, or κ_{nt} = 407 W/(m·K). This value is more than a factor of 3 higher than that obtained by the rule of mixture and, taking into account a large uncertainties in the values involved in the estimation, is in a reasonable agreement with the value of (300 ± 20) W/(m·K) obtained for individual MWNT, using 3-ω method [35]. In fact, it is a compromising value between very high TC (κ > 3000 W/(m·K)) reported in [14] for individual MWNTs, and more than an order of magnitude lower (25 W/m·K) than our value, in dense bundles of aligned MWNTs reported in [13].

The VANT array can also be presented as a 'composite' with environmental atmosphere as a 'matrix'. In normal conditions, the thermal conductivity of the air (κ_m = 0.026 W/(m·K)) can be neglected, then Equation (3) of the rule of mixture to estimate the TC of individual VANT simplifies into (7)

$$\kappa_{nt} \approx \kappa_c / \Phi. \quad (7)$$

Assuming the same Φ = 0.03 as before, this gives an estimate $\kappa_{nt} \approx$ 121 W/(m·K).
Similarly (6) simplifies into (8)

$$\kappa_{nt} \approx \kappa_c \, (3/\Phi - 2), \quad (8)$$

to give the TC of individual VANT $\kappa_{nt} \approx$ 358 W/(m·K) within the effective medium model. Both estimates of the TC of individual VANT in the virgin array are very close to the similar estimates from the data in ER/VANT composites. We consider this fact as evidence of the reliability of the experimental data reported above, though the theoretical analysis needs further improvement.

A modest TC value of individual CNTs estimated from both approaches of rule of mixtures and effective media, compared with the highest reported earlier, can be due to two possible reasons. One is a short length or height of a fraction of tubes compared the sample thickness which can be considered as an extrinsic reason. In this case, an additional heat resistance appears due to the space between the tubes ends and the tubes ends and the surface filled by polymer. The second reason can be different tubes defects, including twinning and crossing of the tubes; formation of sprouts of thinner tubes; and local disordering in tube shells ordering [36], which leads to an additional scattering in the phonons propagation. This reason can be classified as an intrinsic factor. Comparison of the TC data in ER/VANTs composite and in pure VANTs arrays, where there is no additional heat resistance due to surface polymer islands filling the gap between the tube ends and the sample surface, shows that TC in the pure VANTs array is even smaller than in the ER/VANTs composite. This observation proves that the extrinsic factor does not play a decisive role in the weakening of the TC in the ER/VANTs composite. Instead, the intrinsic defects can do this. Moreover, we can state that the polymer matrix makes a kind of bridge between tube endings and healthy parts of the tubes with high conductivity to surpass the defects with high resistivity. A large interface thermal resistance across the nanotube-matrix interface causes a significant degradation in the thermal conductivity enhancement, even for the case with ultrahigh intrinsic thermal conductivity and aspect ratio of the carbon nanotubes embedded is predicted [37] as observed recently in nanotube suspensions.

The results of TC in ER/HANTs could be considered as a way to measure the transversal heat transport in CNTs, i.e., perpendicular to the tube axis. As a simplest approach to describe the heat transport in this case is the series model, where the conductance is limited by a series of a transverse resistance of CNTs ($1/\kappa_{x,nt}$) and that of the matrix ($1/\kappa_m$) with the contribution proportional to the corresponding volume fractions [20]. However, this approach does not work in our case of ER/HANTs composites. Indeed, using the data in Table 1, the composite resistance $1/\kappa_c$ = 0.7 to 1.04 m·K/W is much smaller than the resistance of the polymer matrix $(1 - \Phi)/\kappa_m \approx$ 3.7 m·K/W even without a finite contribution of the CNTs resistance. This effect could be interpreted as (1) a modification of the intrinsic conductivity of the polymer matrix by filling it with CNTs; (2) proximity effect, when the gap between CNTs becomes too small that phonons can propagate to the neighboring CNT over the thin layer of the matrix; (3) extrinsic effect due to bending of CNTs and connecting the bottom and top surfaces. At a given stage, we can state that ER/HANTs sample cannot be considered as an ideal film with CNTs oriented strictly parallel to the surface and separated from each other by the matrix media. Evidently, some of the CNTs are inclined, tilted, or bent, making contact between each other, surfing up to the surface and serving a kind of short-circuits for the heat conductance between back and front surface of the sample. However, an additional study is required to form more solid experimental basis to answer whether the first two reasons can be of importance, say, the intrinsic conductivity of polymer can also change to contribute to the overall conductivity.

4.2. TC Simulations

Heat propagation in the inhomogeneous PM-VANT media was simulated, using COMSOL Multiphysics code applying several approximations, using a model which we call the coaxial cylinder (CC) model. A simplified geometry of the unit cell in the CC model is shown in Supporting Information, Figure S1a. In the model, CNT was substituted by a homogeneous fiber, thus ignoring the internal structure of the CNTs. The simulation is performed in a unit cell consisting of the coaxial cylinders, the fiber, and surrounding polymer, with the cylinders height being equal to the sample thickness, the radius of the fiber being equal to the external radius of the CNTs in the experiment, and the volume of the surrounding polymer cylinder corresponding to the volume of the unit cell in the composite. We assume that the laser pulse energy uniformly absorbed in a thin layer with the thickness of the order of light absorption length of about 50 nm at the bottom surface, i.e., well within the 5 μm graphite coating. This justifies that we ignore the absorption depth distribution, taking the step-like increase of the temperature at the bottom and start the heat propagation right after the pulse duration of 0.3 ms. The magnitude of the step is small, of the order of 1–5 °C, in order to avoid nonlinearities in heat propagation. The parameters of the system assumed in the calculation were as follows: polymer thermal conductivity 0.2 W/(m·K); polymer density 1200 kg/m^3; polymer heat capacity 1200 J/(kg·K); fiber thermal conductivity 300 W/(m·K) (also calculations were done with 3000 W/(m·K)); fiber density 2230 kg/m^3; fiber heat capacity 700 J/(kg·K). Simulation shows that the heat propagates very fast in the fiber and slows in the polymer according to the thermal conductivity. The dynamics of the temperature flow within the model is illustrated in Dyn-heat-prop. The temperature increase at the top surface depends on the difference in the thermal conductivity of the fiber and polymer and on the thermal resistivity on the fiber/polymer interface. The simulation shows that the temperature distribution over fiber becomes uniform immediately during the pulse duration, while it only starts to increase at the bottom of the surrounding polymer. The heat from the fiber also starts to propagate through the interface to the surrounding matrix with the rate, depending on the thermal resistivity of the interface. It is important to note that the detector cannot follow the 2D variation of the surface temperature field, but measures the average temperature over the sample surface.

Dynamics of the average temperature evolution at the top surface is presented in Figure 5, calculated for the model imitated the sample of 100 nm thickness, 250 nm unit cell diameter and 50 nm VANT diameter, corresponding to 4% of VANT concentration in the compound which is close to the concentration in VANT/ER samples in the study.

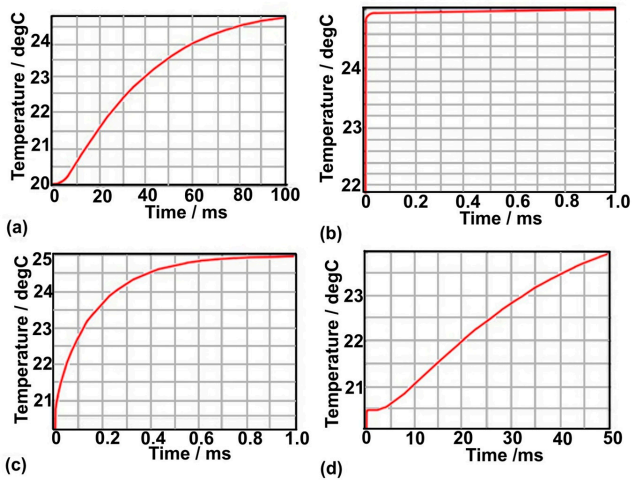

Figure 5. Calculated time variation of the average temperature at the top surface: (**a**) the mean temperature of the top surface of the polymer without fiber; (**b**) the mean temperature of the top surface of the fiber; (**c**) the mean temperature of the composite PM+fiber with zero thermal resistance at the interface PM/fiber; (**d**) the same as (c), but with infinite thermal resistance at the interface.

A sharp rise of the temperature at the fiber top, Figure 5b, contrasting with the slow rise in the case of pure polymer, Figure 5a, reflects the difference in the thermal conductivity of fiber and polymer (note two order of magnitude difference in the time scales). To compare the time scale of the experimental dynamics with simulated ones in pure ER case, we have to take into account the difference in thickness. If we apply Equation (1), than the experimental $t_{1/2}$ (1.8 mm) = 4.1 s for L = 1.8 mm can be reduced to 0.1 mm to obtain $t_{1/2}$ (0.1mm) = 12.6 ms. This half-time is of the same order of magnitude as $t_{1/2}$ (0.1mm) $\approx$ 30 ms obtained in simulation, Figure 5a. The disparity by a factor of 2.4, besides the experimental uncertainties, the uncertainties in model parameters and oversimplifications of the assumptions, can be also be due to inaccuracy in Equation (1). Assuming the proportion $t_{1/2} \sim L^n$, to match the 30 ms instead of 12.6 ms of the experimental half-time, the exponent is to be n = 1.7 instead of n = 2 in Equation (1). Further quantification of the heat propagation dynamics and comparison with in the experimental dynamics in pure VANTs array is unreasonable because of propagation progressing too quickly along the tube/fiber. The temperature almost saturates before the laser pulse ends, see, Figure S1b. Indeed, if we reduce, following Equation (1), $t_{1/2}$ = 10.7 ms for VANT + graphite sample with thickness of 0.59 mm to L = 0.1 mm, we get $t_{1/2}$ = 0.31 ms which is the same as 0.3 ms of laser pulse duration, assuming that both laser heating and heat propagation act simultaneously, requiring a different approach to describe the process.

For the VANT/ER composites, the dynamics strongly depend on the thermal resistivity of the interface between nanotube and polymer matrix. If the interface between the CNT external surface and polymer matrix does not impose any barrier for heat exchange between these two highly different media then, besides the heat transfer from the bottom to the top of the CNTs, there is a heat flow from hot CNT side surface to the polymer matrix, resulting in the averaging of upper surface temperature increase with an intermediate rate between the case of infinite interface heat resistivity, Figure 5d, and pure CNTs array, Figure 5b. The time dependence Figure 5d shows also an additional feature, a step-like temperature rise at the starting point, corresponding to a highly nonuniform temperature distribution, when the fiber ends are seen as hot spots due to high TC surrounded by a relatively cold polymer matrix surface.

The short rise time in Figure 5d represents the very high rate of the heat transfer through the tubes, while the height of the step is determined by the relative area of the tubes. The following slow heating of the surface in the time scale comparable with that for pure polymer matrix, Figure 5a, reflects a lack of the heat contribution from the hot fiber in the case of infinite CNT/matrix contact resistivity.

Reducing, in accordance with Equation (1), $t_{1/2}$ = 13.2 ms for ER/VANT sample with L = 0.56 mm, see Table 1, to the thickness L = 0.1 mm, we get $t_{1/2}$ = 0.42 ms. Comparing this half-time with the predicted rate of the temperature increase in Figure 5, we conclude that the experimental dynamics are much slower than those for composite with zero thermal CNT/matrix contact resistivity with $t_{1/2} \approx$ 0.08 ms, Figure 5c, but much faster than the dynamics with infinite resistivity with $t_{1/2} \approx$ 20 ms, Figure 5c. Thus exploring details of the temperature rise dynamics can give important information on the properties of the CNT/matrix interface.

5. Conclusions

The development of polymer-CNT composites with a certain thermal conductivity and acceptable set of other functional properties is a very important field of research. Currently, however, there is a large scatter, both in theoretical and experimental data on the TC in polymer-CNTs composites. In this paper, we demonstrate that the laser flash analysis can give reliable information on the average thermal conductivity of the composite samples. Different ER/CNTs composites were investigated with taunit (TNC), randomly aligned (RANTs), vertically aligned nanotubes (VANTs), and horizontally aligned nanotubes (HANTs) as fillers in the PNCs. For the reference, the TC of as-grown VANTs array was investigated as well.

It was observed that the measured values for ER/TNC and ER/RANTs were the same within the error bars as for ER. A sharp increase of the thermal conductivity, by a factor of 19, compared with pure

ER, was observed in ER/VANTs composite across the sample thickness and, hence, predominately along the MWNTs axis. We underline that this enhancement was obtained with as-grown VANTs array without any pretreatment like densification or high temperature annealing before making the composite which is important for future applications. In ER/VANTs PNC, the heat transfer can be considered as a parallel heat propagation along the tubes and the matrix with averaging the temperature over the sample surface. Knowing the CNTs volume fraction, TC of individual CNTs was estimated, which is a compromising value between very high TC ($\kappa > 3000$ W/(m·K)) reported in [14] for individual MWNTs, and low (25 W/(m·K)) value in dense bundles of aligned MWNTs reported in [13]. The analysis of extrinsic and intrinsic reasons for weakening the TC compared with the highest value reported in the literature showed that mainly intrinsic reasons—like different tube defects, formation of sprouts of thinner tubes, and local disordering in tube shells ordering—must be responsible for this divergence.

The results of TC in ER/HANTs, where the enhancement by a factor of 5 was obtained, is used to analyze the transversal heat transport across CNTs. The heat conductance is analyzed both as propagation along a series of the heat resistances, including a transverse resistance of CNTs and that of the matrix with the contributions proportional to the corresponding volume fractions. Analysis showed that the series model could not be applied, since the composite resistance is smaller than the resistance of the polymer matrix even without a finite contribution of the CNTs resistance. The effect is ascribed predominantly to the extrinsic reasons due to orientation spread of HANTs. Instead of being ideally arranged parallel to the surface separated by a highly resistive matrix, HANTs are in fact inclined, tilted, bent, making contact between each other, surfing up to the surface and serving a kind of short-circuit for the heat conductance between back and front surface of the sample.

Simulations of the heat propagation illustrate benefits in study the dynamics of the temperature rise at the sample surface in the inhomogeneous anisotropic composite with a drastically different thermal conductivity of the constituents. In particular, the heat resistivity for a finite heat transport in radial direction from hot CNT side surface to cold matrix can, in principal, provide information on the bonding type and strength at the CNT/polymer interface.

Supplementary Materials: The following are available online at www.mdpi.com/2504-477X/1/1/6/s1, Figure S1: (a) Geometry of the unit cell, consisting of the fiber and surrounding polymer in a volume proportion as estimated from the experimental data analysis; (b) a momentary temperature distribution in the cell as calculated with the zero interface thermal resistivity at 40 μs after laser flash start.

Acknowledgments: The help of A.V. Makunin and N.B. Akimov on different stages of the work is highly acknowledged. The work is supported by the Program of MSU Development and Russian Foundation for Basic Research (RFBR) (grant # 14-02-01230a).

Author Contributions: Ekaterina Vorobyeva synthesized samples of carbon nanotubes and composites based on them; Irina Makarenko and Alexey Kepman performed the experiments on the measurement of thermal conductivity and modeling; and Nikolay Chechenin made the analysis of the results. All authors wrote the paper.

Conflicts of Interest: The authors declare no conflict of interest.

References

1. Berber, S.; Kwon, Y.K.; Tománek, D. Unusually high thermal conductivity of carbon nanotubes. *Phys. Rev. Lett.* **2000**, *84*, 4613–4616. [CrossRef] [PubMed]
2. Zhong, H.; Lukes, J.R. Thermal conductivity of single-wall carbon nanotubes. In Proceedings of the IMECE04, ASME International Mechanical Engineering Congress and Exposition, Anaheim, CA, USA, 13–20 November 2004; IMECE2004-61665. pp. 1–9.
3. Osman, M.A.; Srivastava, D. Temperature dependence of the thermal conductivity of single-wall carbon nanotubes. *Nanotechnology* **2001**, *12*, 21–24. [CrossRef]
4. Maruyama, S. Molecular dynamics simulation of heat conduction of a finite length single-walled carbon nanotube. *Microscale Thermophys. Eng.* **2003**, *7*, 41–50. [CrossRef]
5. Padgett, C.W.; Brenner, D.W. Influence of chemisorption on the thermal conductivity of single-wall carbon nanotubes. *Nano Lett.* **2004**, *4*, 1051–1053. [CrossRef]

6. Moreland, J.F.; Freund, J.B.; Chen, G. The disparate thermal conductivity of carbon nanotubes and diamond nanowires studied by atomistic simulation. *Microscale Thermophys. Eng.* **2004**, *8*, 61–69. [CrossRef]
7. Ren, C.; Zhang, W.; Xu, Z.; Zhu, Z.; Huai, P. Thermal conductivity of single-walled carbon nanotubes under axial stress. *J. Phys. Chem. C* **2010**, *114*, 5786–5791. [CrossRef]
8. Che, J.; Çagin, T.; Goddard, W.A., III. Thermal conductivity of carbon nanotubes. *Nanotechnology* **2000**, *11*, 65–69. [CrossRef]
9. Hone, J.; Whitney, M.; Piskoti, C.; Zettl, A. Thermal conductivity of single-walled carbon nanotubes. *Phys. Rev. B* **1999**, *59*, R2514. [CrossRef]
10. Hone, J.; Llaguno, M.C.; Nemes, N.M.; Johnson, A.T.; Fischer, J.E.; Walters, D.A.; Casavant, M.J.; Schmidt, J.; Smalley, R.E. Electrical and thermal transport properties of magnetically aligned single wall carbon nanotube films. *Appl. Phys. Lett.* **2000**, *77*, 666–668. [CrossRef]
11. Yu, C.; Shi, L.; Yao, Z.; Li, D.; Majumdar, A. Thermal Conductance and Thermopower of an Individual Single-Wall Carbon Nanotube. *Nano Lett.* **2005**, *5*, 1842–1846. [CrossRef] [PubMed]
12. Pop, E.; Mann, D.; Wang, Q.; Goodson, K.; Dai, H. Thermal conductance of an individual single-wall carbon nanotube above room temperature. *Nano Lett.* **2006**, *6*, 96–100. [CrossRef] [PubMed]
13. Yi, W.; Lu, L.; Zhang, D.L.; Pan, Z.W.; Xie, S.S. Linear specific heat of carbon nanotubes. *Phys. Rev. B* **1999**, *59*, R9015–R9018. [CrossRef]
14. Kim, P.; Shi, L.; Majumdar, A.; McEuen, P.L. Thermal transport measurements of individual multiwalled nanotubes. *Phys. Rev. Lett.* **2001**, *87*, 215502. [CrossRef] [PubMed]
15. Fujii, M.; Zhang, X.; Takahashi, K. Measurements of thermal conductivity of individual carbon nanotubes. *Phys. Stat. Sol.* **2006**, *243*, 3385–3389. [CrossRef]
16. Shaikh, S.; Li, L.; Lafdi, K.; Huie, J. Thermal conductivity of an aligned carbon nanotube array. *Carbon* **2007**, *45*, 2608–2613. [CrossRef]
17. Bauhofer, W.; Kovacz, J.Z. A review and analysis of electrical percolation in carbon nanotube polymer composites. *Compos. Sci. Technol.* **2009**, *69*, 1486–1498. [CrossRef]
18. Chechenin, N.G.; Chernykh, P.N.; Vorobyeva, E.A.; Timofeev, O.S. Synthesis and electroconductivity of epoxy/aligned CNTs composites. *Appl. Surf. Sci.* **2013**, *275*, 217–221. [CrossRef]
19. Sihn, S.; Ganguli, S.; Roy, A.K.; Qu, L.; Dai, L. Enhancement of through-thickness thermal conductivity in adhesively bonded joints using aligned carbon nanotubes. *Compos. Sci. Technol.* **2008**, *68*, 658–665. [CrossRef]
20. Han, Z.; Fina, A. Thermal conductivity of carbon nanotubes and their polymer nanocomposites. A review. *Prog. Polym. Sci.* **2011**, *36*, 914–944. [CrossRef]
21. Mamunya, Y.; Boudenne, A.; Lebovka, N.; Ibos, L.; Candau, Y.; Lisunova, M. Electrical and thermophysical behaviour of PVC-MWCNT nanocomposites. *Compos. Sci. Technol.* **2008**, *68*, 1981–1988. [CrossRef]
22. Biercuk, M.J.; Llaguno, M.C.; Radosavljevic, M.; Hyun, J.K.; Johnson, A.T.; Fischer, J.E. Carbon nanotube composites for thermal management. *Appl. Phys. Lett.* **2002**, *80*, 2767. [CrossRef]
23. Moisala, A.; Li, Q.; Kinloch, I.A.; Windle, A.H. Thermal and electrical conductivity of single- and multi-walled carbon nanotube-epoxy composites. *Compos. Sci. Technol.* **2006**, *66*, 1285–1288. [CrossRef]
24. Marconnet, A.M.; Yamamoto, N.; Panzer, M.A.; Wardle, B.L.; Goodson, K.E. Anisotropic thermal diffusivity characterization of aligned carbon nanotube-polymer composites. *J. Nanosci. Nanotechnol.* **2007**, *7*, 1581–1588. [CrossRef]
25. Marconnet, A.M.; Yamamoto, N.; Panzer, M.A.; Wardle, B.L.; Goodson, K.E. Thermal conduction in aligned carbon nanotube-polymer nanocomposites with high packing density. *ACS Nano* **2011**, *5*, 4818–4825. [CrossRef] [PubMed]
26. Carbon Nanomaterial "Taunit". Available online: http://www.rusnanonet.ru/goods/20235/ (accessed on 15 June 2017).
27. Makunin, A.V.; Chechenin, N.G.; Serdyukov, A.A.; Bachurin, K.E.; Vorobyeva, E.A. Technological characteristics of the processes of carbon nanostructure production by the methods of plasma-arc and gas-pyrolytic deposition. *Inorg. Mater. Appl. Res.* **2011**, *2*, 252–255. [CrossRef]
28. Chen, H.; Roy, A.; Baek, J.-B.; Zhu, L.; Qua, J.; Dai, L. Controlled growth and modification of vertically-aligned carbon nanotubes for multifunctional applications. *Mater. Sci. Eng.* **2010**, *70*, 63–91. [CrossRef]
29. Singh, C.; Shaffer, M.S.P.; Windle, A.H. Production of controlled architectures of aligned carbon nanotubes by an injection chemical vapor deposition method. *Carbon* **2003**, *41*, 359–368. [CrossRef]

30. Cowan, R.D. Pulse method of measuring thermal diffusivity at high temperatures. *J. Appl. Phys.* **1963**, *34*, 926–927. [CrossRef]
31. Neidhardt, F. *When and How Must Samples Be Coated during LFA Measurements*; Application Note 066; NETZSCH-Gerätebau GmbH: Selb, Germany, 2009.
32. Kim, S.-K.; Kim, Y.-J. Determination of apparent thickness of graphite coating in flash method. *Thermochim. Acta* **2008**, *468*, 6–9. [CrossRef]
33. Bouillonnec, J.; Bernhart, G.; Pinault, M.; Olivier, P.; Mayne-LHemit, M. Thermal conductivity enhancement of vertically aligned long nanotube carpet reinforced thermoset composites. In Proceedings of the 18th International Conference on Composite Structures, Lisbon, Portugal, 15–18 June 2015; Rep. #8071. p. 34.
34. Nan, C.W.; Shi, Z.; Lin, Y.; Li, M. A simple model for thermal conductivity of carbon nanotube-based composites. *Chem. Phys. Lett.* **2003**, *375*, 666–669. [CrossRef]
35. Choi, S.U.S.; Zhang, Z.G.; Yu, W.; Lockwood, F.E.; Grulke, E.A. Anomalous thermal conductivity enhancement in nanotube suspensions. *Nano Lett.* **2006**, *6*, 1589–1593. [CrossRef] [PubMed]
36. Chechenin, N.G.; Chernykh, P.N.; Vorobyeva, E.A.; Dutka, M.V.; Vainshtein, D.I.; De Hosson, J.Th.M. Structure phases of Fe-nanoparticles in vertically aligned multi-walled carbon nanotubes. *J. Surf. Investig. X-ray Synchrotron Neutron Tech.* **2015**, *9*, 1044–1055. [CrossRef]
37. Nan, C.W.; Shi, Z.; Lin, Y.; Li, M. Interface effect on thermal conductivity of carbon nanotube composites. *Appl. Phys. Lett.* **2004**, *85*, 3549. [CrossRef]